J Nanostruct 9(1): 41-50, Winter 2019

RESEARCH PAPER

Optical and Nano Structural Properties of Hematite (α-Fe_2O_3) Nanorods Interacting with Bovine Serum Albumin (BSA)Protein Solution

Ali Ramzannezhad[1], Ali Bahari[1,], Pooria Gill[2]*

[1]*Department of solid state Physics, University of Mazandaran, Babolsar, Iran*

[2]*Nanomedicine Group, Immunogenetics Research Center, Mazandaran University of Medical Sciences, Sari, Iran*

ARTICLE INFO

Article History:
Received 11 October 2018
Accepted 14 December 2018
Published 01 January 2019

Keywords:
Bovine Serum Albumin (BSA)
CTAB
Hematite Nanorods
Hydrothermal Method
Optical Properties

ABSTRACT

Hematite (α-Fe_2O_3) nanorods were synthesized by hydrothermal method using Cetyltrimethylammonium bromide (CTAB) as a surfactant agent. To study optical, nanostructural properties, and to control the morphology and shape of nanorods, 0.025 mol L^{-1}, 0.05 mol L^{-1} and 0.1 mol L^{-1} concentration of CTAB were used. Moreover, the effect of interaction between bovine serum albumin (BSA) A9418-5G protein solution and hematite nanorods was investigated. Fourier transform infrared spectroscopy (FTIR), transmitting electron microscopy (TEM), X-Ray Diffraction (XRD), Energy Dispersive X-Ray Spectroscopy (EDS) and UV-vis spectroscopy were used to characterize α-Fe_2O_3 nanorods. The samples prepared by the interaction of BSA protein and hematite nanorods did not representa rod shape because the electrostatic interaction between CTAB and BSA would cause the nanorods to have a limited capacity for carrying protein. Hematite nanorods obtained from 0.025 mol L^{-1} of CTAB showed a maximum length of 25-30 nm. However, BSA protein solution falsification of rod shape particles increased. The results showed that BSA protein could affect the shape of hematite nanorods and their aggregation, and formspherical structures as well.

How to cite this article
Ramzannezhad A, Bahari A, Gill P. Optical and Nano Structural Properties of Hematite (α-Fe_2O_3) Nanorods Interacting with Bovine Serum Albumin (BSA) Protein Solution. J Nanostruct, 2019; 9(1): 41-50. DOI: 10.22052/JNS.2019.01.006

INTRODUCTION

In recent years, one of the most important applications of magnetic nanorods in diagnosing diseases, which are mainly done by biopsy [1], blood detection [2] and medical imaging [3] methods. These methods are unhelpful in the first stage of the disease, expensive and not easily accessible to many people [4-5]. So, we need to look for a method that is both cost-effective and also has the sensitivity and accuracy of the diagnosis. For this purpose, we use the interaction of magnetic nanorod with BSA aqueous solution in which the albumin is known as a diagnostic biomarker of kidney disease. The interaction of BSA with nanorods can be a model for designing a Magnetic nanobiosensor [6-7]. The magnetic nanobiosensor with fast, accurate and more efficient diagnosis would prevent much healthcare cost. This cost-effective and accurate diagnostic method with high sensitivity could also detect first signals of the disease [8]. In this paper, we discuss the synthesis and characterization of Hematite (α-Fe_2O_3) nanorods before and after interaction with BSA. Various methods were proposed for the synthesis of hematite nanorods, mostly based on chemical methods. Some of the most important ones include: thermal decomposition [9], wet chemical [10], hydrothermal [11], template mediated [12], hydrolysis [13], sol-gel [14] and co-precipitation [15-16]. Until recently, hydrothermal method was the most common approach for the synthesis of hematite nanorods [17-19]. In the

* *Corresponding Author Email: a.bahari@umz.ac.ir*

present work, hydrothermal method was used in which CTAB acted as a surfactant agent at room temperature and interacted with hematite nanorods in BSA aqueous solution. Experimental analysis revealed that BSA would conjugate with inorganic molecules, binding in different directions and changing the morphology and optical properties of hematite nanorods after interaction [22-24].

MATERIALS AND METHODS

Materials

Iron (ш) chliride ($FeCl_3$), sodium hydroxide (NaOH), Cetyl trimethylammonium bromide (CTAB), Phosphate-buffered saline (PBS), and bovine serum albumin(BSA) A9418-5G were all purchased from Sigma-Aldrich and used without further purification.

Synthesis of hematite nanorods

To synthesize hematite nanorods, 0.25 mol L^{-1} of $FeCl_3$ solution was added into a beaker, followed by a dropwise addition of 8.5 mL of NaOH (2mol L^{-1}) and 8.0 mL of deionized water (DIW) under vigorous magnetic stirring at room temperature. Similarly, in a separate beaker, CTAB of different concentrations (0.025, 0.05 and 0.1 mol L^{-1}) was created. Two solutions were slowly mixed while stirring continuously. Then, the resulted transparent mixture was transferred to an autoclave with a capacity of 60 mL, where it was tightly sealed. The sample was heated to 150 °C and kept in an isothermal state for 6.0 h. Subsequently, the samples were cooled to room temperature naturally. The product was filtered and washed with deionized water for three times. PBS pill was solved in 200 cc of deionized water (DIW) to prepare PBS. It was then added to nanorod solution with the same volume of collected deionized water. To prepare the interaction, 0.4, 0.8, 1.6, 3.2 and 6.4 mg per mLconcentration of BSA to PBS solution and hematite nanorods were combined. The resulting interaction solution was saved for further analysis.

Materials Characterization

UV-visible spectroscopy of synthesized magnetic nanorods

Optical properties of hematite nanorods were evaluated using UV–Vis spectrophotometer (GBC Cintra 101), with DIW as dispersive medium. First, distilled water was added to two cuvettes regarded as reference and sample within the system. Scanning the baseline, the wavelength range was adjusted from 200 to 800 nm. In the next step, both reference and sample cuvettes were kept outside. The sample was diluted to 50% and then poured back into its cuvette. Then, it was put in the right place inside the device to be scanned from 200 to 800 nm.

X-ray powder diffraction of hematite nanorods

X-ray powder diffraction (XRD) pattern of as-prepared sample was measured using (GBC-MMA 007) X-ray diffractometer. The diffractograms were recorded with 0.02° step size i (speed of 10 deg/min) radiation over a 2θ range of 10°–80°.

FTIR spectroscopy of synthesized hematite nanorods

Potassium bromide was used as the background to measure FT-IR in 1730 Infrared Fourier Transform Spectrometer (Perkin-Elmer). First, the synthesized powder was completely mixed with potassium bromide since KBr would not be absorbed in the IR region. To make the pill ready to draw FTIR graph,a press device was used.

Energy Dispersive X-Ray Spectroscopy (EDS)

Energy Dispersive X-Ray Spectroscopy (EDS) analysis was used to determine the chemical composition, weight percent (Wt%) and atomic percent (At%) of the elements in each of the compounds (Mira 3-XMU).

Table 1. Compared hydrothermal method with other methods in fabrication of rod-shaped Hematite (α-Fe_2O_3) Iron Oxide Nanoparticles.

The method used by others	The advantage of hydrothermal method	Ref.
Template Mediated	Higher quality and the longer length of the nanorods	[25]
Solvothermal	Simple and less costly	[26]
metal–organic chemical vapor deposition	Low temperature and control of reaction in the formation of nanorods	[27]
Sol-Gel	Little time process and fewer precursor	[28]
Wet chemical	Less reaction and cost-effectiveness in terms of cost	[29]

Transmission electron microscopy of synthesized hematite nanorods

The morphology of solution samples without any changes in their preparation was examined by transmission electron microscopy (TEM, Philips CM30, 150 kV).

RESULTS AND DISCUSSION

Fig. 1 shows UV-Vis spectroscopy of hematite nanorods fabricated with different amounts of CTAB at room temperature (RT). CTAB could affect the shape of hematite nanostructures, causing the products to reach nanorod morphology. The sample prepared without CTAB could form nanoparticle structure (see Fig.1-a), with one peak located at 250 nm, and wavelength of 200–800 nm. However, regarding other amounts of CTAB (0.025, 0.05 and 0.1, mol L^{-1}), the absorption band of hematite nanorods mainly located between 210-250 nm and 350-380 nm (see Fig.1, b-d), and CTAB could influence the formation of hematite nanorods. Figs. 2a-2c show optical absorption spectra of hematite nanorods prepared with constant amounts of CTAB and different volumes of DIW to obtain nanorods with more regular shapes. As can be seen, at 0.025 mol L^{-1} of CTAB with 5, 10 and 15 mL DIW, there were two sharp peaks around 250 and 420 nm in the visible region indicating that the product could exhibit the rod shape of hematite nanostructures.

Xia and colleagues [30] showed a possible relationship between UV-vis spectrum and

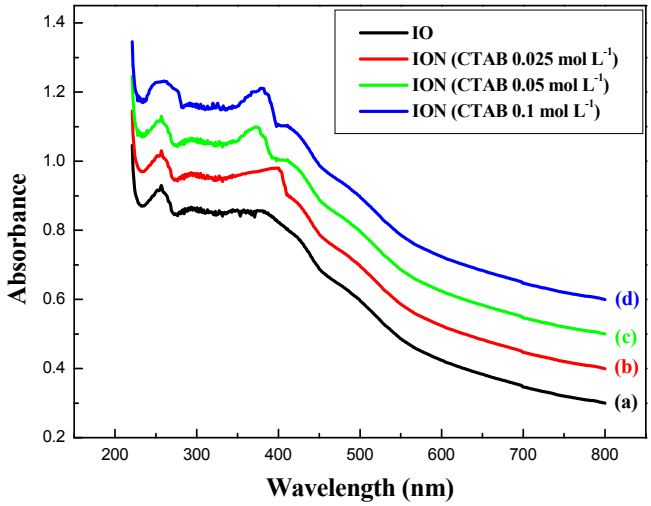

Fig. 1. UV–vis spectra of hematite nanorods prepared at RT with: (a) without CTAB, (b) 0.025 mol L^{-1} (c) 0.05 mol L^{-1} and (d) 0.1 mol $L^{-1}$of CTAB.

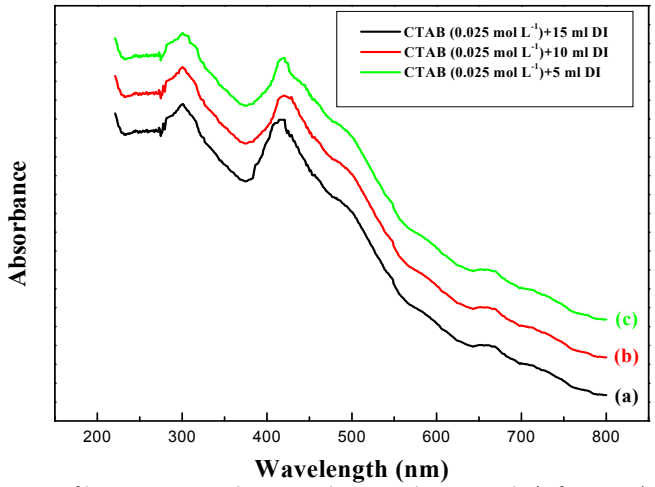

Fig. 2. UV–vis absorption spectra of hematite nanorods prepared at RT with 0.025 mol L^{-1} of CTAB in (a) 15 mL DIW, (b) 10 mL DIW and (c) 5 mL DIW.

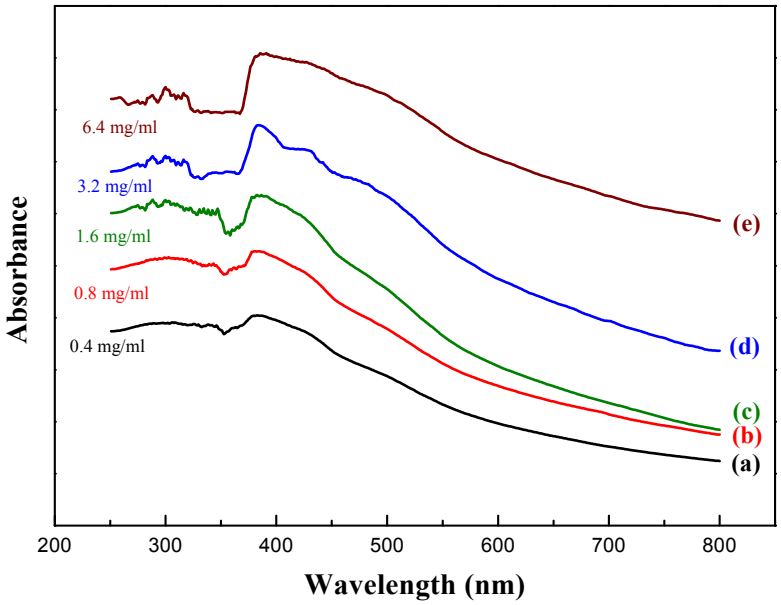

Fig. 3. UV–vis absorption spectra of hematite nanorods prepared at RT with (a) 0.4 mg/ml, (b) 0.8 mg/ml, (c) 1.6 mg/ml, (d) 3.2 mg/ml and (e) 6.4 mg/ml of BSA solution.

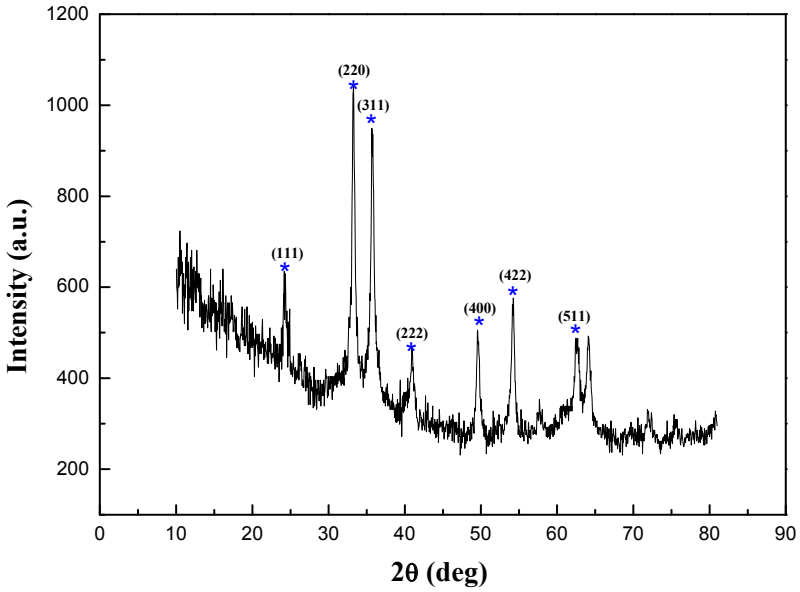

Fig. 4. XRD pattern of as-prepared hematite nanorods at RT.

morphology of nanostructures. The interaction between BSA protein and hematite nanorods would cause the peak at 300 nm to disappear, and the peak at 400 nm to show a red shift after adding BSA solutions of 0.4, 0.8, 1.6, 3.2 and 6.4 mg per ml (see Fig.3, b-f) concentrations. The interaction could change the structure of hematite nanorods due to the presence of a peak around 400 nm and the nanoparticles having spherical shape, which was in agreement with TEM microscopic analysed images.

XRD was used to study crystalline phase of the hematite nanorod powder. Fig. 4 shows XRD pattern of the powder obtained from 0.025 molof L^{-1} CTAB at RT. The sharp peaks would indicate that the crystal structure of hematite nanorods

was related to (111), (220), (222), (311), (400), (422), and (511) Miller indices, corresponding to the formation of hematite phase based on the 73-0603 standard card [31]. The average size was calculated with Scherrer equation, according to which the full width at half maximum (FWHM) of peak 220 was about 15 nm [32,33]:

$$D=0.89\lambda/\beta\cos\vartheta \quad (1)$$

Where λ = 0.154 nm, and θ is the reflection angle.

FTIR analysis was done to study the structure and measures of chemical species of produced particles. Fig. 5 shows FTIR spectra of hematite nanorods before interacting with albumin. FTIR pattern of hematite nanorods obtained from 0.025, 0.05 and 0.1 mol L^{-1} concentration of CTAB at RT indicated stretching and bending vibration

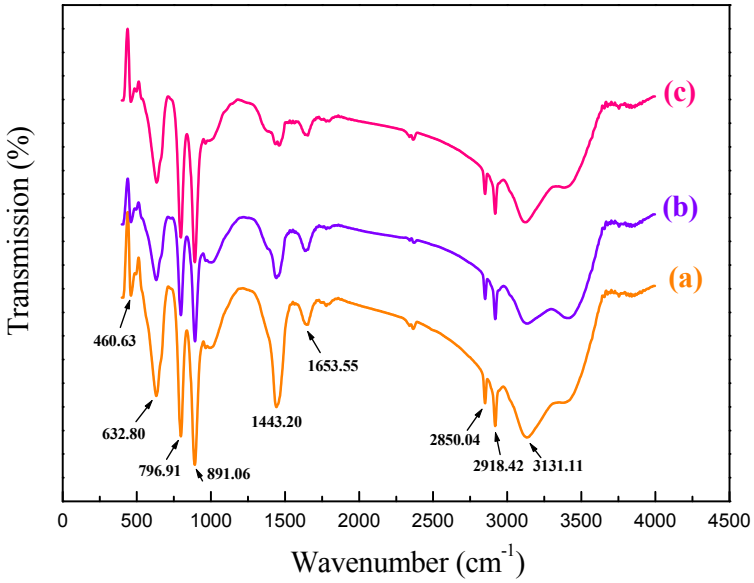

Fig. 5. FTIR spectra of hematite nanorods prepared with (a) 0.025, (b) 0.05, and (c) 0.1 mol L^{-1} concentration of CTAB at RT.

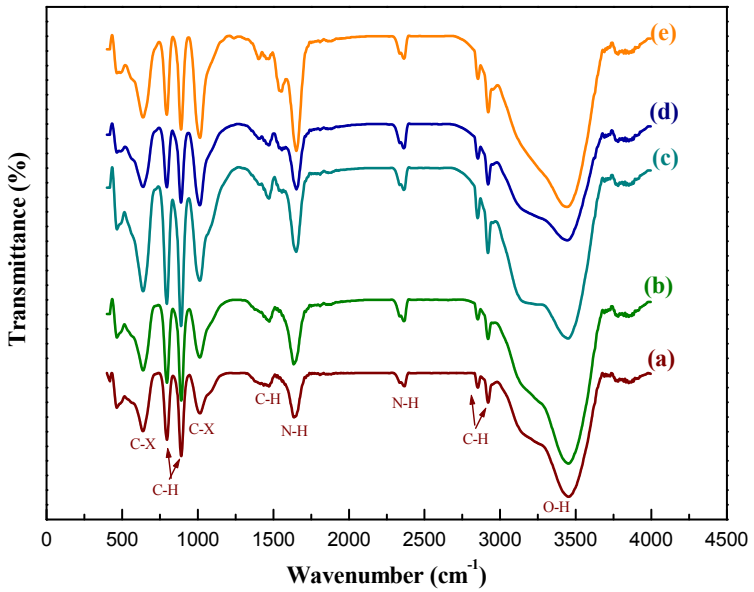

Fig. 6. FTIR spectraof hematite nanorods prepared (a) without albumin, (b) 0.4 mg/ml, (c) 0.8 mg/ml, (d) 1.6 mg/ml, (e) 3.2 mg/ml and (f) 6.4 mg/ml concentration of BSA.

modes. Figs. 5a-5c show that, in symmetrical vibrations, infrared spectroscopy bands were 1280-1400 cm^{-1}, and in asymmetrical vibrations, they were 1440-1660 cm^{-1}[34]. The band of around 1443.20 cm^{-1} indicated the presence of CH_3 groups [35]. FTIR spectra contained several small bands in 2850.04, 2918.42 and 3131.11 cm^{-1} regions. These bands could be assigned either to the carbonyl group or to asymmetric vibrations of unidentified carboxylate [36-37]. On the other hand, the stretching vibration showed a weak IR band of 1660-1640 cm^{-1} that would overlap with carbonyl vibrations [38]. Bands less than 650 cm^{-1} also represented the Fe-O vibration mode [39]. Vibrations of hematite became apparent at 460.63 cm^{-1} and 632.80 cm^{-1}. Adding BSA protein solution to hematite nanorods, some changes in Fourier transform infrared spectroscopy absorption of BSA/α-$Fe_2O_3$was observed, compared to α-Fe_2O_3 nanorods (see Fig.6, a-e). Fig. 6 illustrates a mixture of nanorods and protein formed with 0.4 mg/ml, 0.8 mg/ml, 1.6 mg/ml, 3.2 mg/ml and 6.4

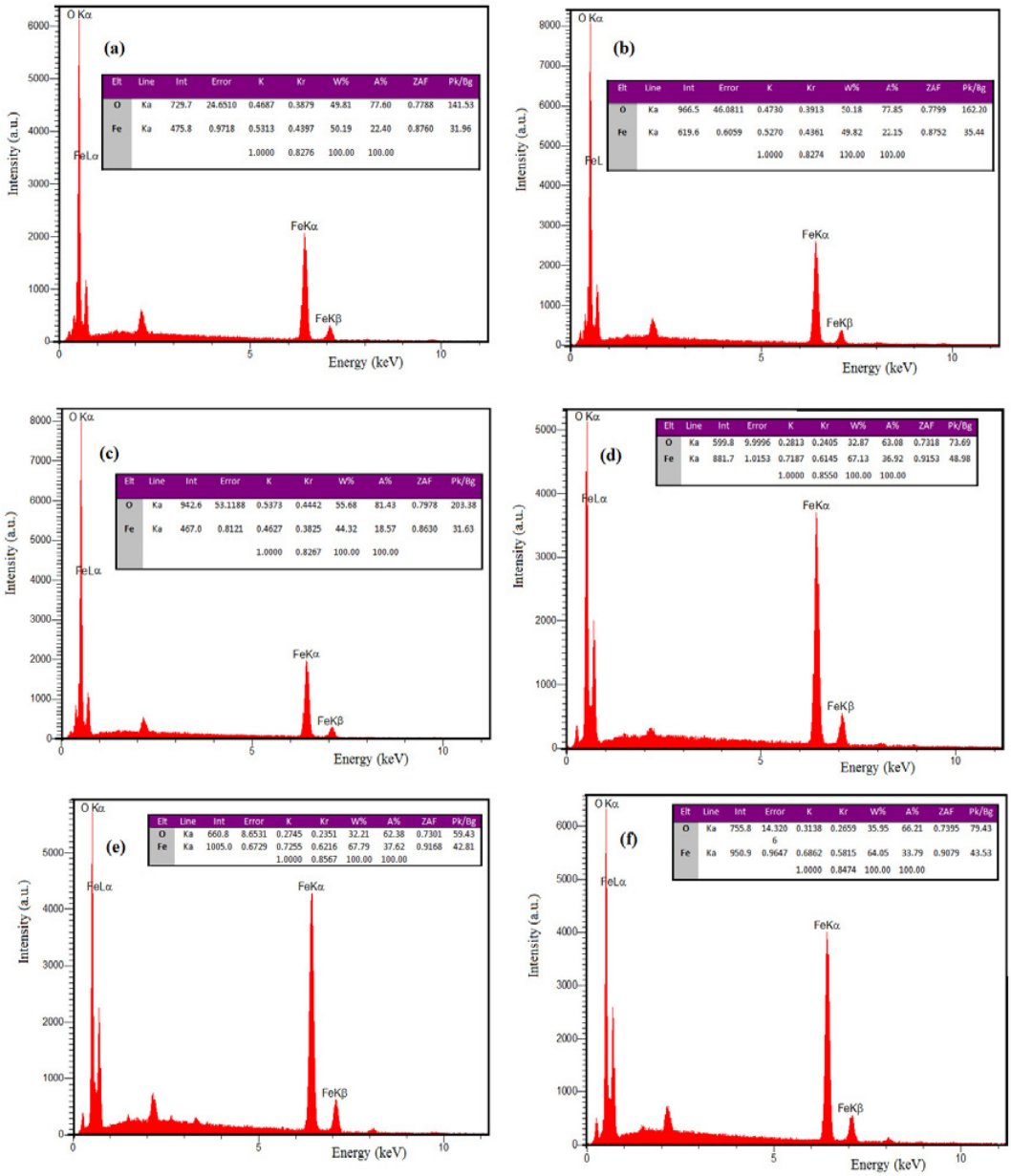

Fig. 7. Elemental analyses of hematite nanorods prepared with (a) 0.025 mol L^{-1} CTAB, (b) 0.05 mol L^{-1} CTAB, (c) 0.1 mol L^{-1} of CTAB, (d) 0.4 mg/ml BSA, (e) 0.8 mg/ml BSA and (f) 1.6 mg/ml BSA by Energy Dispersive X-Ray Spectroscopy (EDS).

mg/ml of BSA solution. Increasing the volume of BSA to 6.4 mg/ml at 2800-2900 cm^{-1}, nochanges in chemical structures were seen. The main bonds in BSA/α-Fe_2O_3were formed at 1013.28 and 1647.59 cm^{-1}. These bonds corresponded to vibrational modes of Iron to oxygen atoms, linking to proteins on CTAB surface.

We used elemental analysis to prove the existence of iron element in the samples. Fig. 7 shows the Energy Dispersive X-Ray Spectroscopy (EDS) spectrum of hematite nanorods prepared with 0.025, 0.05 and 0.1 mol L^{-1}concentration of CTAB and elemental analysis of hematite nanorods after interacting with BSA in concentrations of 0.4, 0.8 and 1.6 mg/ml. As can be seen in the insert of Fig. 7, the results indicated the presence of Fe and O in the hematite samples. The sample with 0.8 mg/ml of BSA have more Wt% of Fe than samples with 0.025, 0.05 and 0.1 mol L^{-1}concentration of CTAB.

TEM helped to obtain more morphological details of nanostructures. Figs. 8a-8c show TEM images of hematite nanorods prepared with 0.025, 0.05 and 0.1 mol L^{-1}concentration of CTAB, and their distribution using Digimizer software. The results showed the formation of uniform nanorod structures. The average length of hematite nanorods in TEM images was calculated using Digimizer software. The distribution graph of nanorods is presented in Figs. 10a-10c. As shown in Fig. 10, the average lengths of hematite nanorods were about 25-30, 50-55and 25-30 nm in 0.025, 0.05 and 0.1 mol L^{-1}concentration of CTAB, respectively.

Fig. 9 shows TEM images of hematite nanorods after interacting with BSA. On average, the surface charge of CTAB was positive, but in albumin the surface charge was negative. Both positive and negative charges interacted electrostatically. When protein concentration was more than CTAB, electron microscope images of samples showed changes in morphology and aggregation of the nanorods.The averagelengths of hematite nanorods were about 25-30, 5-50and 30-40 nm at 0.4 mg/ml, 0.8 mg/ml and 1.6 mg/ml concentration of BSA, respectively.

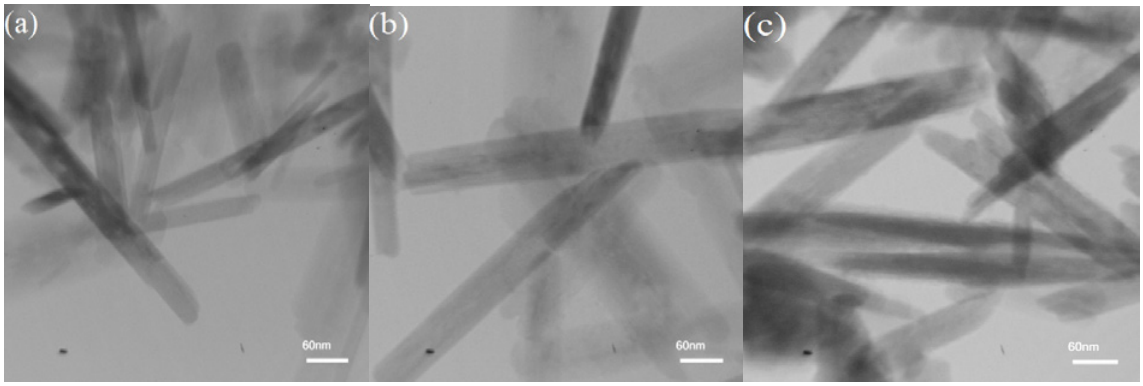

Fig. 8. TEM images of hematite nanorods prepared with (a) 0.025 mol L^{-1}, (b) 0.05 mol L^{-1} and (c) 0.1 mol L^{-1} of CTAB.

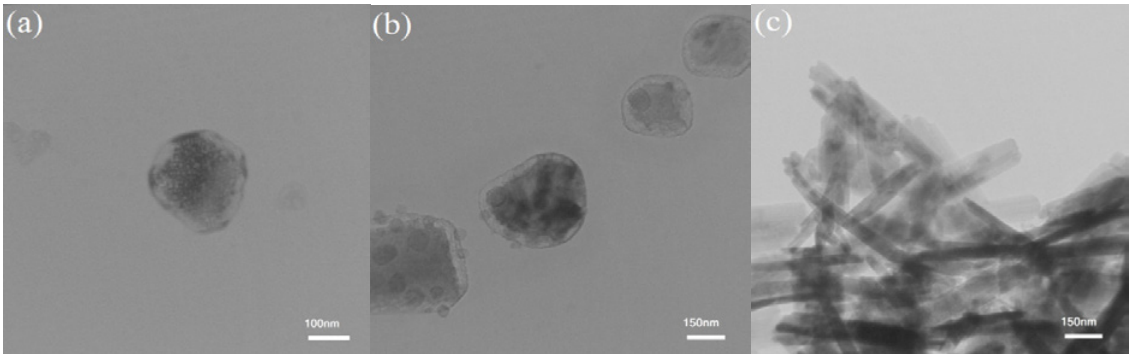

Fig. 9. TEM imagesof hematite nanorods prepared at (a) 0.4 mg/ml, (b) 0.8 mg/ml and (c) 1.6 mg/ml concentration of BSA.

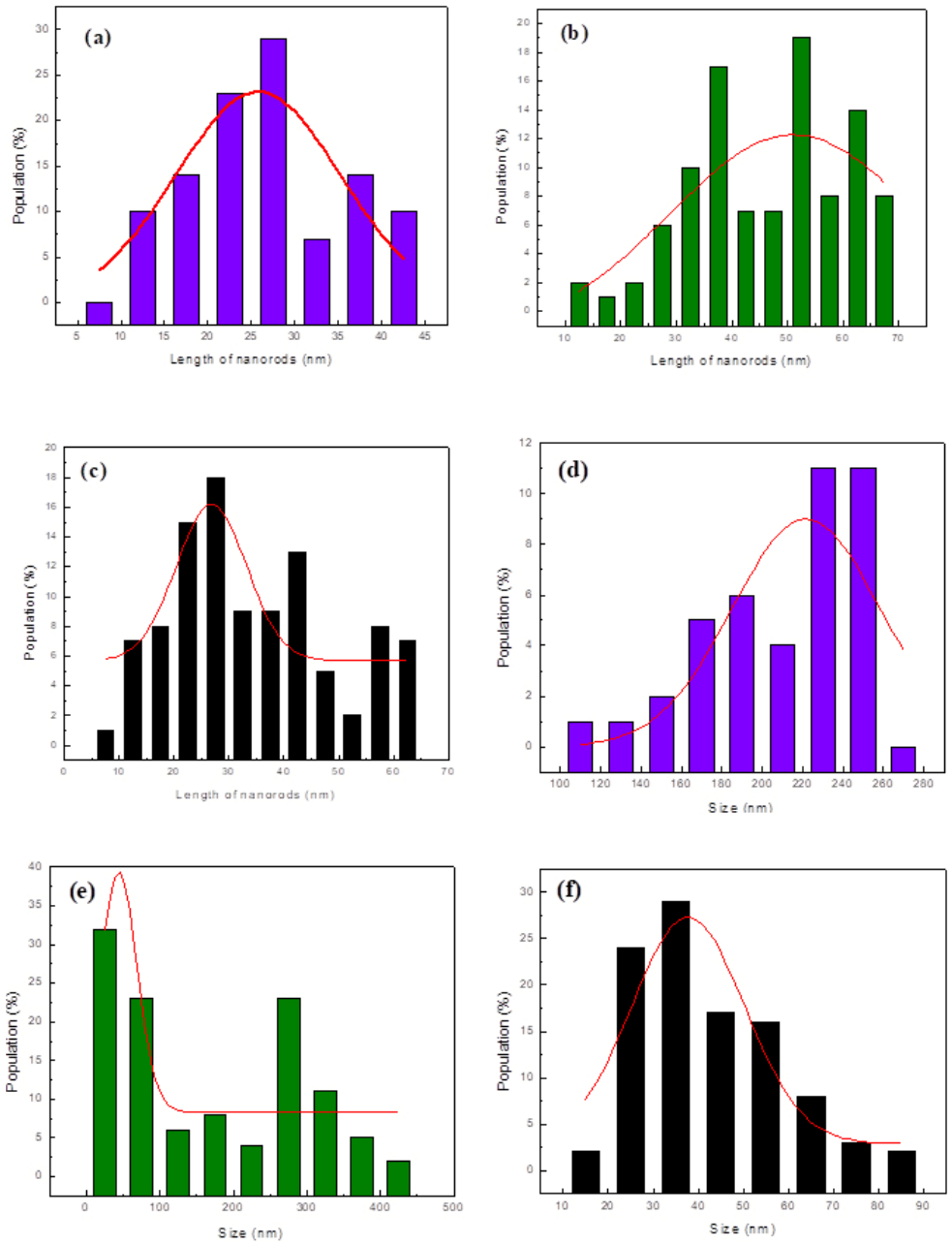

Fig. 10. Size distribution of hematite nanorods prepared with (a) 0.025 mol L^{-1} CTAB, (b) 0.05 mol L^{-1} CTAB, (c) 0.1 mol L^{-1} of CTAB, (d) 0.4 mg/ml BSA, (e) 0.8 mg/ml BSA and (f) 1.6 mg/ml BSA.

CONCLUSION

Hematite (α-Fe_2O_3) nanorods were synthesized using hydrothermal method with CTAB as a surfactant agent at different molar ratios. The interaction between BSA protein and hematite nanorods could affect the morphology and optical properties of hematite nanostructures. The size and shape of hematite nanorods could change with different amounts of BSA solution at room temperature. UV-vis spectroscopy revealed two main peaks before interaction, which showed the formation of nanorods. While adding BSA protein solution to nanorods, peaks disappeared and optical properties of samples changed. In addition, the microscopic technique parallel to absorption spectroscopy could confirm the formation of hematite nanorods and their spherical shape after interacting with BSA protein.

CONFLICT OF INTERESTS

The authors declare that there is no conflict of interests regarding the publication of this paper.

REFERENCES

1. Ito T, Ishikawa E, Ito M. Lumbar artery injury following renal biopsy. Clinical and Experimental Nephrology. 2015;20(1):145-6.
2. Bogdanov M, Matson WR, Wang L, Matson T, Saunders-Pullman R, Bressman SS, et al. Metabolomic profiling to develop blood biomarkers for Parkinson's disease. Brain. 2008;131(2):389-96.
3. Teo BM, Young DJ, Loh XJ. Magnetic Anisotropic Particles: Toward Remotely Actuated Applications. Particle & Particle Systems Characterization. 2016;33(10):709-28.
4. Su X, Tan MJ, Li Z, Wong M, Rajamani L, Lingam G, et al. Recent Progress in Using Biomaterials as Vitreous Substitutes. Biomacromolecules. 2015;16(10):3093-102.
5. Shahmiri MR, Bahari A, Karimi-Maleh H, Hosseinzadeh R, Mirnia N. Ethynylferrocene–NiO/MWCNT nanocomposite modified carbon paste electrode as a novel voltammetric sensor for simultaneous determination of glutathione and acetaminophen. Sensors and Actuators B: Chemical. 2013;177:70-7.
6. Page TR, Hayamizu Y, So CR, Sarikaya M. Electrical detection of biomolecular adsorption on sprayed graphene sheets. Biosensors and Bioelectronics. 2012;33(1):304-8.
7. Zeng S, Tang K, Li T. Controlled synthesis of α-Fe2O3 nanorods and its size-dependent optical absorption, electrochemical, and magnetic properties. Journal of Colloid and Interface Science. 2007;312(2):513-21.
8. Narayanan TN, Shaijumon MM, Ajayan PM, Anantharaman MR. Synthesis of High Coercivity Core–Shell Nanorods Based on Nickel and Cobalt and Their Magnetic Properties. Nanoscale Research Letters. 2009;5(1):164-8.
9. Park J, Koo B, Hwang Y, Bae C, An K, Park J-G, et al. Novel Synthesis of Magnetic Fe2P Nanorods from Thermal Decomposition of Continuously Delivered Precursors using a Syringe Pump. Angewandte Chemie. 2004;116(17):2332-5.
10. Bahari A, Roeinfard M, Ramzannezhad A. Characteristics of Fe3O4/ZnO nanocomposite as a possible gate dielectric of nanoscale transistors in the field of cyborg. Journal of Materials Science: Materials in Electronics. 2016;27(9):9363-9.
11. Liang S, Zhu S, Chen Y, Wu W, Wang X, Wu L. Rapid template-free synthesis and photocatalytic performance of visible light-activated SnNb2O6nanosheets. J Mater Chem. 2012;22(6):2670-8.
12. Salavati-Niasari M, Davar F, Mahmoudi T. A simple route to synthesize nanocrystalline nickel ferrite (NiFe2O4) in the presence of octanoic acid as a surfactant. Polyhedron. 2009;28(8):1455-8.
13. Han BS, Uhm YR, Kim GM, Rhee CK. Novel Synthesis of Nanorod ZnO and Fe-Doped ZnO by the Hydrolysis of Metal Powders. Journal of Nanoscience and Nanotechnology. 2007;7(11):4158-60.
14. Asadi S, Abdizadeh H, Vahidshad Y. Effect of Crystalline Size on the Structure of Copper Doped Zirconia Nanopaticles Synthesized via Sol-Gel. J Nanostruct. 2012;2(2):205-12.
15. Ghaani M, Saffari J. Synthesis of CuFe2 O4 Nanoparticles by a new co-precipitation method and using them as Efficient Catalyst for One-pot Synthesis of Naphthoxazinones. J Nanostruct. 2016;6(2):172-8.
16. Kolen'ko YV, Kovnir KA, Gavrilov AI, Garshev AV, Frantti J, Lebedev OI, et al. Hydrothermal Synthesis and Characterization of Nanorods of Various Titanates and Titanium Dioxide. The Journal of Physical Chemistry B. 2006;110(9):4030-8.
17. Razi F, Zinatloo-Ajabshir S, Salavati-Niasari M. Preparation and characterization of HgI2 nanostructures via a new facile route. Materials Letters. 2017;193:9-12.
18. Li Z, Lai X, Wang H, Mao D, Xing C, Wang D. Direct hydrothermal synthesis of single-crystalline hematite nanorods assisted by 1,2-propanediamine. Nanotechnology. 2009;20(24):245603.
19. Polsongkram D, Chamninok P, Pukird S, Chow L, Lupan O, Chai G, et al. Effect of synthesis conditions on the growth of ZnO nanorods via hydrothermal method. Physica B: Condensed Matter. 2008;403(19-20):3713-7.
20. Zeng Y, Hao R, Xing B, Hou Y, Xu Z. One-pot synthesis of Fe3O4 nanoprisms with controlled electrochemical properties. Chemical Communications. 2010;46(22):3920.
21. Sun S, Zeng H, Robinson DB, Raoux S, Rice PM, Wang SX, et al. Monodisperse MFe2O4(M = Fe, Co, Mn) Nanoparticles. Journal of the American Chemical Society. 2004;126(1):273-9.
22. poner J, Hobza P. DNA base amino groups and their role in molecular interactions: Ab initio and preliminary density functional theory calculations. International Journal of Quantum Chemistry. 1996;57(5):959-70.
23. Saptarshi SR, Duschl A, Lopata AL. Interaction of nanoparticles with proteins: relation to bio-reactivity of the nanoparticle. Journal of Nanobiotechnology. 2013;11(1):26.
24. Zinatloo-Ajabshir S, Salehi Z, Salavati-Niasari M. Preparation, characterization and photocatalytic properties of Pr2Ce2O7 nanostructures via a facile procedure. RSC Advances. 2016;6(109):107785-92.
25. An K, Hyeon T. Synthesis and biomedical applications of hollow nanostructures. Nano Today. 2009;4(4):359-73.
26. Muraliganth T, Murugan AV, Manthiram A. Nanoscale networking of LiFePO4 nanorods synthesized by a microwave-solvothermal route with carbon nanotubes for lithium ion batteries. Journal of Materials Chemistry. 2008;18(46):5661.
27. Cha HG, Kim CW, Kim YH, Jung MH, Ji ES, Das BK, et al. Preparation and characterization of α-Fe2O3 nanorod-thin film by metal–organic chemical vapor deposition. Thin Solid Films. 2009;517(5):1853-6.
28. Woo K, Lee HJ, Ahn JP, Park YS. Sol–Gel Mediated Synthesis of Fe2O3 Nanorods. Advanced Materials. 2003;15(20):1761-4.
29. Zhang Y, Fugane K, Mori T, Niu L, Ye J. Wet chemical synthesis of nitrogen-doped graphene towards oxygen reduction electrocatalysts without high-temperature pyrolysis. Journal of Materials Chemistry. 2012;22(14):6575.
30. Xia Y. Nanomaterials at work in biomedical research. Nature Materials. 2008;7(10):758-60.
31. Gou X, Wang G, Kong X, Wexler D, Horvat J, Yang J, et al. Flutelike Porous Hematite Nanorods and Branched Nanostructures: Synthesis, Characterisation and Application for Gas-Sensing. Chemistry - A European Journal. 2008;14(19):5996-6002.
32. Bahari A, Ramzannejad A. NANOSTRUCTURAL PROPERTIES

OF La2O3/HfO2 GATE DIELECTRICS. International Journal of Modern Physics B. 2012;26(14):1250080.
33. Zinatloo-Ajabshir S, Salavati-Niasari M, Zinatloo-Ajabshir Z. Nd 2 Zr 2 O 7 -Nd 2 O 3 nanocomposites: New facile synthesis, characterization and investigation of photocatalytic behaviour. Materials Letters. 2016;180:27-30.
34. Fu H, Quan X. Complexes of fulvic acid on the surface of hematite, goethite, and akaganeite: FTIR observation. Chemosphere. 2006;63(3):403-10.
35. Zinatloo-Ajabshir S, Salavati-Niasari M, Zinatloo-Ajabshir Z. Facile size-controlled preparation of highly photocatalytically active praseodymium zirconate nanostructures for degradation and removal of organic pollutants. Separation and Purification Technology. 2017;177:110-20.
36. Soflaee F, Farahmandjou M, Firoozabadi TP. Polymer-Mediated Synthesis of Iron Oxide (Fe_2O_3) Nanorods. Chinese Journal of Physics. 2015;53(4):178-86.
37. Zinatloo-Ajabshir S, Mortazavi-Derazkola S, Salavati-Niasari M. Sono-synthesis and characterization of Ho2O3 nanostructures via a new precipitation way for photocatalytic degradation improvement of erythrosine. International Journal of Hydrogen Energy. 2017;42(22):15178-88.
38. Scarano D, Zecchina A, Bordiga S, Geobaldo F, Spoto G, Petrini G, et al. Fourier-transform infrared and Raman spectra of pure and Al-, B-, Ti- and Fe-substituted silicalites: stretching-mode region. Journal of the Chemical Society, Faraday Transactions. 1993;89(22):4123.
39. Si J-C, Xing Y, Peng M-L, Zhang C, Buske N, Chen C, et al. Solvothermal synthesis of tunable iron oxide nanorods and their transfer from organic phase to water phase. CrystEngComm. 2014;16(4):512-6.